M Siccinio et al.

Analytical models for the evaluation of thermal loads on divertor and first wall in DEMO

Analytical models for the evaluation of thermal loads on divertor and first wall in DEMO

M. Siccinio[a*], L. Barbato[b], E. Fable[a], K. Lackner[a], F. Maviglia[c,d],
A. Scarabosio[a], A. K. Stegmeir[a], R. P. Wenninger[a,d], H. Zohm[a]

[a] *Max Planck Institut für Plasmaphysik, Boltzmannstr. 2, 85748 Garching bei München, Germany*
[b] *Consorzio CREATE, Univ. Cassino e del Lazio meridionale, Via G. Di Biasio, 43 I-03043 Cassino, Italy*
[c] *Consorzio CREATE, Univ. Napoli Federico II - DIETI, 80125 Naples, Italy*
[d] *EUROfusion Consortium, PPPT Department, Boltzmannstr. 2, 85748 Garching bei München, Germany*

Abstract

In the frame of the currently ongoing pre-conceptual design analysis phase for the reactor DEMO, two simple investigations connected to the evaluation of the thermal loads on plasma-facing components (PFCs) have been carried out. In the first one, the role of "filaments", or "blobs", which have been shown in recent experiments to cause a significative enhancement of the radial transport in the scrape-off layer (SOL) when the divertor collisionality exceeds a critical value [1], is addressed. Such radial transport leads in turn to an additional particle and energy flux onto the first wall (FW), which might become critical for a machine like DEMO where the technological limits on the FW-heat flux are quite strict. This aspect has been investigated by means of a field-line tracing code employing a realistic DEMO magnetic equilibrium [2]. It is shown that, with reasonable assumptions, filaments might indeed carry a significant fraction of the maximum tolerable heat load, this circumstance pointing out their importance for a correct evaluation of the power distribution on the PFCs. In the second part, a 0D model to determine the detachment degree on the divertor plate by given upstream conditions and impurity concentrations is presented. The model, mainly based on previous works of Igitkhanov [3, 4, 5], contains heat conduction and convection, SOL and divertor radiation and a simplified balance for the neutrals. The aim is to be quick - thus necessarily simplistic - in order to provide a tool which is appropriate either for system codes or more in general to be employed in the preliminary design phase of the reactor DEMO.

Keywords: DEMO, filaments, first wall, detachment, system codes

1 Introduction

The numerous criticalities associated to the feasibility of a future nuclear fusion power plant are strictly connected one to the other. Thus, a comprehensive approach to the design of the prototypical machine DEMO is mandatory, especially in the currently ongoing pre-conceptual design analysis phase. From

---

*Contact: mattia.siccinio@ipp.mpg.de

this point of view, the realisation of models which are at the same time simple but able to capture the most relevant aspects of the fusion plasma physics is of primary importance. The problem of power exhaust is commonly acknowledged to be a crucial issue for the design of a future nuclear fusion reactor like DEMO [6]. It has for example been observed [7] that, in view of the high power crossing the separatrix [8] and of the relatively small area on which it is supposed to be deposited according to the existing scaling laws [9, 10], it would be impossible for DEMO to operate in an attached divertor regime without largely exceeding the technological limit of 10-15 MW/m^2 of thermal load on the divertor plates [11]. Furthermore, because of the presence of the breeding blanket, the maximum tolerable *local* heat load on the first wall is limited to around 1 MW/m^2 [12], i.e. about one fourth of the corresponding ITER value, although in DEMO a larger power is supposed to be radiated [7, 8]. In this paper, two analytical tools to evaluate the influence of the blobby transport on the FW heat load and to estimate the detachment degree at the divertor plate by given upstream conditions, respectively, are presented. Their simplicity is justified by the requirement of flexibility for an integrated approach to the design of an entire power plant - for example when coupled to a system code like PROCESS [13]. Nevertheless, their accuracy has been tested against more complex and complete physical models.

2 Filamentary Transport in DEMO

2.1 Framework

Blobs - or filaments - are coherent and elongated structures propagating in the SOL which are denser and hotter than the surrounding plasma. Their existence is known since the nineties [14], but only recently they have become an active area of both theoretical and experimental research. Blobs travel along and across the open magnetic field lines and possess the remarkable feature of deviating charged particles, otherwise directed to the divertor, onto the FW. Although the mechanism which originates them has not been fully understood yet, it is experimentally known that they are mostly emitted from the low-field side of the machine into the SOL. Along the magnetic field lines, blobs elongate in both directions (upstream and downstream) with a velocity of the order of the sound speed c_s, but they also exhibit a perpendicular drift, roughly oriented along the major radius coordinate. From a theoretical point of view, an explanation for this drift has been provided for the first time in Ref.[15]. Depending on the total resistivity along the SOL field lines, different propagation regimes have been identified [16, 17]. In particular, in the limit of negligible resistivity, the perpendicular velocity can be estimated as

$$v_\perp \simeq 2c_s \frac{L_\parallel}{R} \frac{\rho_s^2}{\delta_b^2},$$ (1)

thus decreasing with increasing blob size δ_b (here, $L_\parallel$ is the connection length, R is the major radius and ρ_s is the sonic radius). This regime is often referred to as *sheat limited*. In these conditions, the transport associated to the blobs is essentially negligible, as the perpendicular displacement a filament experiences during its travel towards the divertor decreases by increasing amount of particles and energy it contains. In the opposit limit, i.e. when the resistivity is sufficiently high (which in most case implies the detachment of the divertor), filaments propagate following the so called *inertial* regime scaling, namely

$$v_\perp \simeq c_s \sqrt{\tilde{p}\frac{\delta_b}{R}}, \tag{2}$$

where $\tilde{p}$ is the relative amplitude of the pressure fluctuation with respect to the background plasma. This implies that the associated particle transport is now much more effective, as larger blobs are convected quickly and therefore undergo larger displacements (in view of the $\sqrt{\delta_b}$ scaling), possibly striking on the FW very close to the outer midplane. In recent publications, Carralero et al. [1, 18] have shown experimentally the transition between these two propagation regimes to be essentially determined by the collisionality at the divertor plates. In particular, when the condition

$$\Lambda \doteq \frac{L_\parallel/c_{s,Div}}{1/\nu_{e,i,Div}}\frac{m_e}{m_i} > 1, \tag{3}$$

is fulfilled, the perpendicular drift exhibits a dependence on the blob size compatible with Eq.2, following Eq.1 otherwise (in Eq.3, $\nu_{e,i}$ is the electron-ion collision frequency and m_e and m_i are the electron and ion mass, respectively, the subscript Div indicating that all quantities are calculated at the target). The condition $\Lambda > 1$ is not easily achieved in the existing tokamak facilities, as the high density and the low temperature that have to be mantained at the target have negative repercussions on the stability of the discharge. *However, for realistic DEMO conditions, blobs will propagate following the inertial regime scaling law, and therefore the fraction of particle and power transported by blobs onto the FW is expected to be higher than what observed in nowadays tokamaks.* This claim can be easily understood by noting that, in DEMO, $L_\parallel$ will be significantly larger than in present days machines, and at the same time the collisionality at the divertor (because of lower temperature and detachment, which is a necessary condition for DEMO to operate [7]) will be comparable or, more probably, larger. This lets the parameter Λ increase well below unity. Assuming for example a divertor temperature of 2 eV and a plasma density of 3e19 m^{-3}, one finds $\Lambda \sim 100$.

Robust experimental evidences showing that, when $\Lambda > 1$, the *density* profile in the SOL becomes flatter (leading to the formation of the so called "shoulder") are available in the literature, see for example [19, 20] and references therein. This occurrence is explained by the increase of filamentary transport elucidated above. However, no similar evidence has yet been found concerning

the energy transport, the debate on this point remaining on a quite speculative level. Some authors assume the energy transport to remain relatively low [21], whereas other publications claim blobs are able to transport towards the FW a fraction of the power entering the SOL (henceforth P_{SOL}) up to 40% or even more [22, 23, 24]. In spite of our incomplete knowledge, the magnitude of the energy filamentary transport is the most important aspect connected to the presence of blobs in view of the design of DEMO, as P_{SOL} is expected to be pretty high (recall that it has in any case to be higher than the L-H transition threshold), and thus even a small fraction of heat being deviated onto the FW might lead to very high local thermal loads, representing a serious threaten to the integrity of PFCs. In the following analysis, the power fraction carried by blobs is left as a free parameter, a deeper insight on this crucial aspect being expected from shortcoming experimental analysis.

Before discussing the results, we limit ourselves to mention another aspect connected to the presence of blobs which possesses a certain relevance but which will not be considered here, i.e. the enhancement of the sputtering on the first wall. The magnitude of this phenomenon is strictly linked to the temperature of the blobs striking onto the FW, which has not been experimentally determined yet. In addition, the role of the increased flux of particles might be in any case negligible in comparison to the self-sputtering of charged tungsten atoms. An interesting discussion on this topic can be found for example in [25].
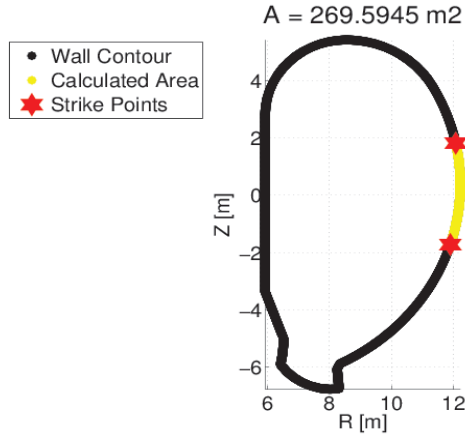

Figure 1: Exemplary visualization of a surface on which the power contained in a blob (here, $\delta_b = 3$ cm and $f_v = 1$) is deposited. A realistic DEMO contour has been employed.
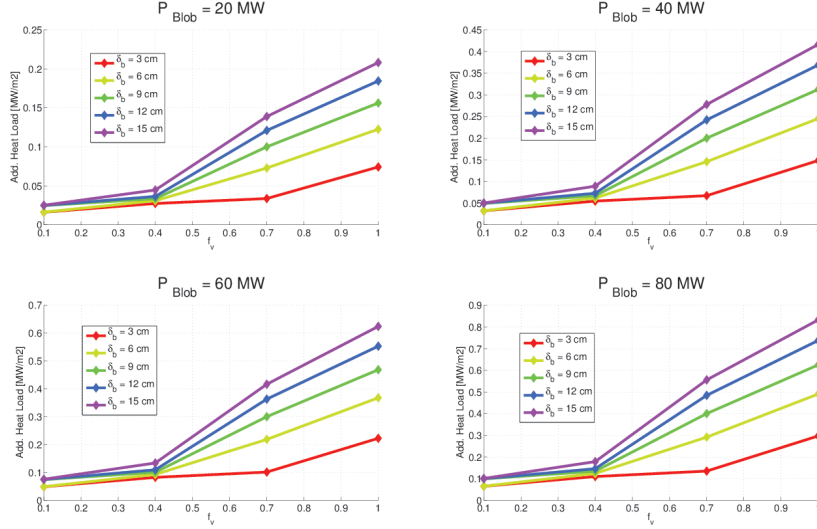
4

Figure 2: Additional heat load on the DEMO first wall due to the filaments for various transported power, blob sizes and f_v-s. In DEMO, the maximum allowable heat load on the FW amounts to 1 MW/m^2 [12].

2.2   Model and Results

The present investigation has been carried out by means of a field-line tracing code [2] which has already been employed for DEMO related investigations [26]. The code is able to follow the trajectory of a single particle along any given magnetic field line using realistic magnetic equilibria (as for example .eqdsk files - a DEMO end of flattop equilibrium has been chosen for the present analysis), thus individuating the strike points on the first wall or on the target plates for lines lying outside the separatrix. In our simulations, all blobs have been initialised on the separatrix at the outer midplane with zero length in the parallel direction, elongating however both upstream and downstream with a velocity equal to c_s. The associated perpendicular velocity is calculated by means of Eq.2 and superposed to the parallel motion. As Eq.2 is known both experimentally and theoretically to be an upper limit rather than an exact prediction (in view of the large amount of physical mechanisms affecting the blob propagation, see e.g. [27]), a corrective factor $0 \leq f_v \leq 1$ is employed. In the future, a careful estimation of f_v in a realistic DEMO geometry will be performed numerically by means of the field-aligned turbulence code Grillix [28], but for the moment this parameter is left as free. Simulations identify for each blob size two strike points (up- and downstream) on the first wall. Assuming toroidal symmetry, this individuates in turn a "ring" on the plasma chamber, whose total area

5

is essentially determined by the position of the two strike points, as shown in Fig.1. A fixed amount of power is supposed to be deposited by filaments on the individuated area. As previously mentioned, no direct experimental measurement of this power as a fraction of P_{SOL} is to our knowledge available. We have therefore considered four values, i.e. 20, 40, 60 and 80 MW (corresponding to 10%-40% for a $P_{SOL} = 200$, MW which is a reasonable DEMO value) and calculated the corresponding heat load for different blob sizes and corrective factors f_v. Results are shown in Fig.2. Obviously, larger blobs deposit on smaller surfaces, as their perpendicular velocity is larger and thus they impact closer to the outer midplane. Note incidentally that the intermittency of the blobby transport has not been taking into account, assuming the frequency of these events to be fast enough to treat the power deposition as quasi-stationary.

This simple analysis shows that, even without being too pessimistic, a significant fraction of the maximum tolerable heat load impacting on the FW might be carried by the enhanced filamentary transport. Dedicated experiments in present machines could provide more information on the actual level of heat transport induced by blob propagation in the inertial regime, consequently allowing better quantitative estimates in view of the design of a future nuclear fusion reactor.

3   0D Divertor Model

3.1   Framework

It has already been observed [6, 7] that it would be impossible for DEMO to operate in an attached divertor regime without greatly exceeding the maximum allowable thermal load on the target plate, this both because of the very large P_{SOL} and of the narrow e-folding length, as already mentioned in the introduction. Thus, a simple model able to predict the onset of the detachment by given upstream conditions is particularly useful for the pre-conceptual design analysis phase. In this second part of our work, such a 0D model is presented, mainly based on previous works of Igitkhanov [3, 4, 5]. The relatively simple set of equations makes this tool particularly appropriate for being employed in system codes, or more in general for the search of optimised design points on a power plant level. In spite of its simplistic approach, justified by the aim of keeping the computational time as short as possible, the model embraces the prominent physical mechanisms determining the onset of detachment (heat convection, heat conduction, flux expansion at the divertor plates, impurity radiation, ionisation and charge exchange), possessing therefore a high flexibility together with a reasonable degree of accuracy.

3.2 Model

A magnetic field line of length $L_\parallel$ connecting the outer midplane to the divertor plate is artificially subdivided into two regions, labelled with I and II. More specifically:

- **Region I**. Herewith, the heat is supposed to be transported along the field line only via *conduction*, assuming constant static pressure. Impurity radiation is present, and the relative concentration of each radiative species $c_{z,j}^I$ (with the index j labelling the species) is supposed to be spatially homogeneous. The region extends from the outer midplane for a distance indicated with L_r.

- **Region II**. This is the *convective* region, which starts from L_r and reaches the target plate. It is characterised by pure convection (assuming Mach number $M = 1$), constant total pressure and impurity radiation, with the relative concentration of the radiative species, $c_{z,j}^{II}$ again supposed to be homogeneous, although not necessarily equal to $c_{z,j}^I$. Its length is denoted with $L_m = L_\parallel - L_r$. The transition between conduction and convection is supposed to take place where the critical temperature T_C is reached. The value of T_C, which is a free parameter in the model, has been fixed at 15 eV, in agreement with the existing literature, see e.g. [29].

The temperature at the plates, indicated with T_{sh}, acts as input for the momentum loss calculation, which in turn determines the degree of detachment. For the sake of simplicity, the influence of the momentum losses on the temperature profile has not been taken into account. In the following, quantities defined at
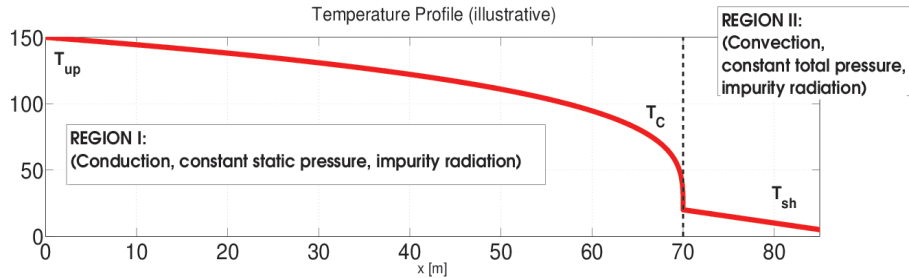

Figure 3: Schematic representation of the field line between outer midplane and target plate. The vertical dashed line has been set at $x = L_r$ to identify the boundary between the conductive and the convective region. The profile represented here is purely illustrative.

the outer midplane are denoted by the subscript *up* and quantities at the interface between the conductive and the convective region with the subscript

I. A further distinction is introduced for quantities defined at the end of the magnetic fieldline *but without having considered momentum losses* , indicated with *sh*, and quantities actually reaching the target plate after the interaction with the neutrals, indicated with the subscript *pl*. Figure 3 schematically depicts the subdivision of the magnetic field line.

Analogously to the well-known two-point-model [30], it is here supposed that the entire particle and energy flux crossing the separatrix be concentrated at the outer midplane. The model consists in seven equations and seven unknowns (T_{up}, q_I, L_r, T_{sh}, q_{sh}, f_m, q_{pl}). The upstream power flux q_{up}, the upstream density n_{up} and the impurity concentrations are required as input. Here, we limit ourselves to write the system of equations without providing a detailed derivation, referring the interested reader to the more complete [31].

$$q_{up}^2 = q_I^2 + 2\chi_0 (n_{up}T_{up})^2 \sum_j c_{z,j}^I \int_{T_C}^{T_{up}} \mathrm{d}T \sqrt{T} l_{z,j}(T) \tag{4}$$

$$L_r = \chi_0 \int_{T_C}^{T_{up}} \mathrm{d}T \frac{T^{5/2}}{q(T)} \tag{5}$$

$$q_I = \frac{\gamma}{2} e n_{up} T_{up} c_{s0} \sqrt{T_C} \tag{6}$$

$$\int_{T_{sh}}^{T_C} \mathrm{d}T \frac{T^{3/2}}{\sum_j c_{z,j}^{II} l_{z,j}(T)} = \frac{n_{up}T_{up}}{\gamma e c_{s0}} L_m \tag{7}$$

$$q_{sh} = \frac{\gamma}{2} e n_{up} T_{up} c_{s0} \sqrt{T_{sh}} \tag{8}$$

$$f_m = 1 - 2 \left(\frac{\alpha_{ps}}{1 + \alpha_{ps}} \right)^{(\alpha_{ps}+1)/2} \tag{9}$$

$$q_{pl} = (1 - f_m) \frac{\gamma}{2 f_x} e n_{up} T_{up} c_{s0} \sqrt{T_{sh}}. \tag{10}$$

Eq.4 describes the energy losses due to radiation in the conductive region [32]. The constant χ_0 is connected to the well-known Spitzer-Härm heat conductivity φ_{SH} via $\varphi_{SH} = \chi_0 T^{5/2}$, whereas the factor γ in Eq.6 and 8 is the commonly employed sheath multiplication factor. Eq.7 is the analogous of Eq.4 for a purely conductive region with M = 1. Observe that, in the limit of no radiating losses in region II, one recovers $T_C = T_{sh}$ and therefore $q_I = q_{sh}$, consistently with the assumption of pure conductive transport. The momentum loss factor f_m - defined as the ratio between the total pressure losses and the upstream total pressure - determines the degree of detachment, $f_m = 0$ corresponding in particular to no detachment and $f_m = 1$ corresponding to a complete loss of particle flux. To determine this parameter, we employ a very simple model, Eq.9, developed by Self and Ewald [33, 34], which possesses the remarkable feature of letting f_m be a function of the temperature T_{sh} only (through the parameter α_{ps}, calculated following [35]). The flux expansion due to the inclination of the target plate with respect to the considered magnetic

field line is accounted for through the factor f_x in Eq.10 (a reasonable value for DEMO is $f_x = 8 - 10$). Note also that every other variation of the flux tube cross section along the magnetic field line has been neglected. Finally, e indicates the electron charge whereas c_{s0} is the sound speed at $T = 1$ eV. The model has been calibrated against a more complex 1D routine [36], providing satisfactory results (again, we have to refer the interested reader to [31]).
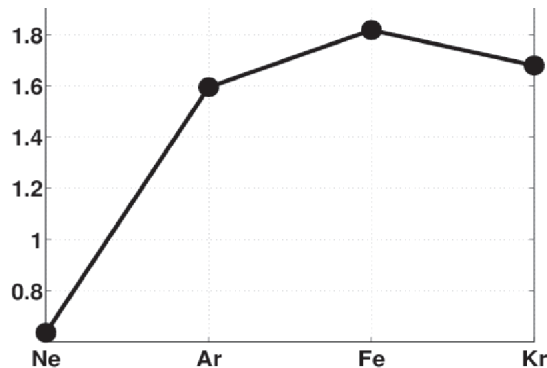
3.3 Application

Figure 4: ASTRA Results: Final value of the fusion power [GW] as a function of the chosen SOL radiating impurity.

The routine has been coupled with the well-known core transport code ASTRA [37, 38] to carry out a preliminary DEMO scenario investigation. The simulations presented here are run employing two species of radiating impurities. In detail, the noble gas xenon, playing the role of main radiative species for the plasma core, is associated to a second atomic species j, which radiates in the SOL/divertor. Xenon is supposed to be puffed at the outer midplane, its concentration in the region one $c_{z,Xe}^I$ being therefore connected to its core concentration in a simplified way through the compression factor $w_{Core,I}^{Xe}$

$$w_{Core,I}^{Xe} \doteq \frac{c_{z,Xe}^{Core}}{c_{z,Xe}^{I}} = 3 \tag{11}$$

Similarly, a compression factor between region I and II is introduced

$$w_{II,I}^{Xe} \doteq \frac{c_{z,Xe}^{II}}{c_{z,Xe}^{I}} = 0.3. \tag{12}$$

This means that the Xe concentration in the core and in the divertor are supposed to be almost equal to one third of the SOL one, where the gas is puffed. The second atomic species j is on the contrary supposed to be injected

9

directly in the divertor, being therefore more concentrated in region II than in region I or in the core. Specifically, we set

$$w_{Core,I}^j \doteq \frac{c_{z,j}^{Core}}{c_{z,j}^I} = 6 \tag{13}$$

and

$$w_{II,I}^j \doteq \frac{c_{z,j}^{II}}{c_{z,j}^I} = 6 \tag{14}$$

Four species j have been considered in the present analysis, namely argon, neon, krypton and iron. ASTRA calculates the density, temperature and fusion power profiles in the core, providing q_{up} and n_{up} to the 0D model, which in turn determines q_{pl}. Impurity concentrations are adjusted until the constraints of $P_{SOL} = 170$ MW (i.e. above the predicted value necessary for the L-H transition, see [8]) and $q_{pl} < 10$ MW/m^2 are simultaneously fulfilled. By virtue of the compression factors, it is impossible to change the SOL radiation without affecting the main plasma and viceversa, thus any modification in the SOL is influencing at the same time the core profiles, which are then updated by ASTRA. The goal of the present investigation consists in determing which impurity combination has the smallest impact on the output fusion power.

The results of the calculations are shown in Fig. 4. As one can observe, it has been impossible to find a solution with neon. In fact, a strong deterioration in the fusion power, Fig.4, takes places without having achieved a sufficient reduction of the heat flux at the target plate, which remains above 10 MW/m^2. This happens as the neon concentration in the main plasma pollutes the core too much in comparison to the little benefits in region I. On the contrary, a solution has been found for argon, krypton and iron, the latter having the obvious problem of not being a gas and therefore being impossible to be puffed. The necessary concentrations for xenon and for the considered SOL radiative species turn out however to be extremely high (more than 20% for argon in region II), clearly indicating that the possibility of confining impurities in the SOL, preventing them to excessively contaminate the main plasma, is of paramount importance for the operation of a future nuclear fusion reactor.

4 Acknowledgments

References

[1] D. Carralero et al., Phys. Rev. Lett. **115**, (2015) 215002

[2] R. Albanese *et al.*, Fus. Sci. and Techn. **68**, 1 (2015)

[3] Yu. Igitkhanov *et al.*, 21st EPS, Montpellier, ECA v.18B, 1994

[4] Yu. Igitkhanov *et al.*, 22th EPS, Bournemouth, ECA v.19C, 1995

[5] Yu. Igitkhanov, KIT Scientific Reports 7661 (2014)

[6] H. Zohm *et al.*, Nucl. Fusion **53**, 073019 (2013)

[7] R. P. Wenninger *et al.*, Nucl. Fusion **54**, 114003 (2014)

[8] G. Giruzzi *et al.*, Nucl. Fusion **55**, 073002 (2015)

[9] T. Eich *et al.*, Phys. Rev. Lett. **107**, 215001 (2011)

[10] T. Eich *et al.*, Nucl. Fusion **53**, 093031 (2013)

[11] G. Federici *et al.*, Fusion Eng. Des. **89** Issue 7-8, 882 (2014)

[12] R. P. Wenninger *et al.*, Nucl. Fusion **55**, 063003 (2015)

[13] M. Kovari *et al.*, Fusion Eng. and Des. **89**, 3054 (2014)

[14] M. Endler, IPP Report III/197 (1994)

[15] S. I. Krasheninnikov, Phys. Letter A **283**, 368 (2001)

[16] J. R. Myra, D. A. Russell and J. A. D'Ippolito, Phys. Plasmas **13**, 112502 (2006)

[17] S. I. Krasheninnikov, D. A. D'Ippolito and J. R. Myra, J. Plasma Physics **74**, 679 (2008)

[18] D. Carralero *et al.*, Nucl. Fusion **54** 123005 (2014)

[19] H. W .Müller *et al.*, J. Nucl. Mater. **463**, 739 (2015)

[20] D. Carralero *et al.*, J. Nucl. Mater. **463**, 123 (2014)

[21] J. A. Boedo *et al.*, Phys. Plasmas **10**, 1670 (2003)

[22] M. V. Umansky *et al.*, Phys. Plasmas **5**, 3373 (1998)

[23] M. Bernert *et al.*, Plasma Phys. Control. Fusion **57**, 014038 (2015)

[24] B. LaBombard *et al.*, Phys. Plasmas **8** Nr. 5, 2107 (2001)

[25] G. Birkenmeier *et al.*, Nucl. Fusion **55**, 033018 (2015)

[26] F. Maviglia *et al.*, Development of DEMO wall heat load specification - Talk presented at 1st IAEA Technical Meeting on Divertor Concepts. Vienna. (2015)

[27] J. Olsen *et al.*, Plasma Phys. Control. Fusion **58** 044011 (2016)

[28] A. K. Stegmeir, PhD Thesis, TU München 2015

[29] A. Leonard *et al.*, Nucl. Fusion **52**, 063015 (2012)

[30] M. Keilhacker. Plasma Physics and Controlled Nuclear Fusion Research, III:183 (1982)

[31] M. Siccinio *et al.*, submitted to Plasma Phys. Control. Fusion

[32] L. L. Lengyel, IPP Report 1/191 (1981)

[33] S. A. Self and H. N. Ewald, Phys. Fluids **9**, 2486 (1966)

[34] C. S. Pitcher and P. C. Stangeby, Plasma Phys. Control. Fusion **39**, 779 (1997)

[35] K. Lackner *et. al*, WPDTT1 - CD02 (unpublished) 2015

[36] A. Kallenbach *et al.*, Plasma Phys. Control. Fusion **58**, 045013 (2016)

[37] G. V. Pereverzev, IPP Report 5/42 (1991)

[38] E. Fable *et al.*, Plasma Phys. Control. Fusion **55**, 124028 (2013)